Stk40 deletion elevates c-JUN protein level and impairs mesoderm differentiation

Received for publication, February 8, 2019, and in revised form, May 7, 2019 Published, Papers in Press, May 15, 2019, DOI 10.1074/jbc.RA119.007840

Jing Hu[‡], Shuang Li[‡], Xiaozhi Sun[‡], Zhuoqing Fang[§], Lina Wang[‡], Feng Xiao[§], Min Shao[§], Laixiang Ge[‡], Fan Tang[‡], Junjie Gu[‡], Hongyao Yu[‡], Yueshuai Guo[¶], Xuejiang Guo[¶], Bing Liao[‡1], and Ying Jin[‡§‖2]

From the [‡]Basic Clinical Research Center, Renji Hospital and Shanghai Key Laboratory of Reproductive Medicine, Department of Histoembryology, Genetics and Developmental Biology, Shanghai Jiao Tong University School of Medicine, 227 South Chongqing Road, Shanghai 200025, China, [§]CAS Key Laboratory of Tissue Microenvironment and Tumor, Shanghai Institute of Nutrition and Health, CAS Center for Excellence in Molecular Cell Science, Shanghai Institutes for Biological Sciences, University of Chinese Academy of Sciences, Chinese Academy of Sciences, 320 Yueyang Road, Shanghai 200032, China, [‖]School of Life Science and Technology, ShanghaiTech University, 100 Haike Road, Shanghai 201210, China, and [¶]State Key Laboratory of Reproductive Medicine, Department of Histology and Embryology, Nanjing Medical University, Nanjing 211166, China

Edited by Joel M. Gottesfeld

Mesoderm development is a finely tuned process initiated by the differentiation of pluripotent epiblast cells. Serine/threonine kinase 40 (STK40) controls the development of several mesoderm-derived cell types, its overexpression induces differentiation of mouse embryonic stem cells (mESCs) toward the extraembryonic endoderm, and *Stk40* knockout (KO) results in multiple organ failure and is lethal at the perinatal stage in mice. However, molecular mechanisms underlying the physiological functions of STK40 in mesoderm differentiation remain elusive. Here, we report that *Stk40* ablation impairs mesoderm differentiation both *in vitro* and *in vivo*. Mechanistically, STK40 interacts with both the E3 ubiquitin ligase mammalian constitutive photomorphogenesis protein 1 (COP1) and the transcriptional regulator proto-oncogene c-Jun (c-JUN), promoting c-JUN protein degradation. Consequently, *Stk40* knockout leads to c-JUN protein accumulation, which, in turn, apparently suppresses WNT signaling activity and impairs the mesoderm differentiation process. Overall, this study reveals that STK40, together with COP1, represents a previously unknown regulatory axis that modulates the c-JUN protein level within an appropriate range during mesoderm differentiation from mESCs. Our findings provide critical insights into the molecular mechanisms regulating the c-JUN protein level and may have potential implications for managing cellular disorders arising from c-JUN dysfunction.

Gastrulation is critical for early mammalian embryonic development, and one of its major tasks is to generate a mesodermal layer between the endoderm and ectoderm. Mesoderm development initiates with differentiation of pluripotent epiblast cells into the primitive streak, which then segregates into the mesoderm layer (1–3). This delicate process is coordinated by multiple key signaling pathways to ensure the correct formation of mesodermal tissues. Among them, bone morphogenesis protein (BMP)[3] and WNT signaling pathways play profound roles to orchestrate mesoderm development (4–6). For instance, *Wnt3*-null mouse embryos lack the primitive streak and mesoderm formation (4). Moreover, WNT signaling is required for the generation of embryonic stem cell (ESC)-derived mesoderm, particularly for the expression of genes related to primitive streak formation and gastrulation *in vivo* (5). Furthermore, induced differentiation of pluripotent stem cells toward the mesodermal fate in monolayer cultures by manipulating WNT and BMP signaling pathways has been achieved *in vitro* (2, 3, 7), highlighting the decisive roles of the two pathways in mesoderm development. However, the molecular mechanisms regulating their activities in mesoderm formation remain incompletely understood.

The transcriptional regulator proto-oncogene c-Jun (c-JUN), encoded by *Jun* gene, acts as a subunit of the activating protein 1 (AP-1) family of transcription factors. By forming a homodimer or heterodimer with other members of the AP-1 family, c-JUN plays important roles in regulating cell proliferation as well as cell migration and oncogenic transformation (8–10). Forced expression of c-JUN in mouse ESCs (mESCs)

This work was supported by National Natural Science Foundation of China Grants 31871373, 31730055, 31301015, and 31200980; Ministry of Science and Technology of China Grant 2016YFA0100100; and Strategic Priority Research Program Grant XDB19020100 of the Chinese Academy of Sciences. The authors declare that they have no conflicts of interest with the contents of this article.

The data discussed in this publication have been deposited in NCBI's Gene Expression Omnibus and are accessible through GEO Series accession number GSE125877.

The mass spectrometric raw data and spectral libraries associated with this manuscript are available from ProteomeXchange with the accession number PXD012579.

This article contains Tables S1–S4.

[1] To whom correspondence may be addressed. E-mail: liaobing@shsmu.edu.cn.

[2] To whom correspondence may be addressed. E-mail: yjin@sibs.ac.cn.

[3] The abbreviations used are: BMP, bone morphogenesis protein; STK40, serine/threonine kinase 40; c-JUN, transcriptional regulator proto-oncogene c-Jun; T, Brachyury; AP-1, activating protein 1; ESC, embryonic stem cell; JNK, c-JUN N-terminal kinase; UPS, ubiquitin–proteasome system; COP1, mammalian constitutive photomorphogenesis protein 1; GO, gene ontology; KO, knockout; CHIR, CHIR99021; MEF, mouse embryonic fibroblast; co-IP, coimmunoprecipitation; CHX, cycloheximide; Dox, doxycycline; DDB1, DNA damage–binding protein-1; TCF, T-cell factor; mESC, mouse ESC; HMG, high mobility group; CEBPβ, CCAAT-enhancer–binding protein β; HA, hemagglutinin; DMEM, Dulbecco's modified Eagle's medium; qRT-PCR, quantitative real-time PCR; TMT, tandem mass tag; ACN, acetonitrile; CDS, coding sequence; GST, glutathione *S*-transferase; DAPI, 4′,6-diamidino-2-phenylindole; DET1, de-etiolated-1.

activated endoderm lineage–related transcriptional factors (*Gata4*/*Gata6*) with the concomitant repression of *Brachyury* (*T*), a mesodermal marker gene (11), whereas the loss of c-JUN function in zebrafish inhibited ventral mesoderm induction (12), implying that the precisely balanced c-JUN level is crucial for mesoderm differentiation. A previous study showed that phosphorylated c-JUN (serine 63 and serine 73) could interact with the HMG-box transcription factor T-cell factor 4 (TCF4) to form protein complexes containing c-JUN, β-catenin, and TCF4 (13). A later study by Gan *et al.* (12) clearly showed that c-JUN is involved in the canonical WNT signaling, dependent on its phosphorylation. Moreover, multiple E3 ligases that add ubiquitin molecules on c-JUN have been unveiled, such as FBW7 (14), ITCH (15), and mammalian constitutive photomorphogenesis protein 1 (COP1) (16). COP1 is a RING-finger E3 ubiquitin ligase. It acts through two distinct regulatory mechanisms, either as an E3 ligase or an adaptor to recruit substrates to DET1-Cullin4 ubiquitin ligase complexes, mediating ubiquitination and degradation of target proteins, such as c-JUN, E26 transformation-specific (ETS) (17), and ETS variant (ETV) (18). c-JUN can bind COP1 directly through a conserved consensus sequence, VP(D/E), located at its C terminus (19). The mutation of the VP sequence into AA disrupts the association between c-JUN and COP1 (16, 19). Remarkably, *Cop1* deficiency stimulates cell proliferation by means of elevating c-JUN protein levels *in vivo* during embryogenesis, and *Cop1*-hypomorphic mice are tumor-prone, in line with the inverse correlation between COP1 and c-JUN proteins in human prostate cancers (20). Therefore, the proper amount of c-JUN is essential for early embryo development, and the ubiquitin–proteasome system (UPS) acts as a potential pathway to reduce c-JUN protein levels.

Serine/threonine kinase 40 (*Stk40*) was originally identified as a direct target gene of OCT4, a pluripotency-associated transcription factor, in mESCs by our laboratory (21). *Stk40*-null mice die at the perinatal stage (22). Further studies unveiled that *Stk40* deletion leads to disorders in adipogenesis (23), myogenesis (24), and erythropoiesis (25). Interestingly, all of these involved cell types are of mesodermal origin. Therefore, we speculated that *Stk40* might participate in the control of early mesoderm development in mouse embryos. Recently, human STK40 was identified as a pseudokinase lacking the ATP-binding property (26). The same study also reported the interaction between STK40 and E3 ligase COP1 in human cells, although the functional consequence of the STK40–COP1 interaction remains unclear.

To address the question of whether STK40 plays a role in mesoderm development, we modified a previously published protocol for mesoderm induction from both wildtype (WT) and *Stk40*-knockout (KO) mESCs by activating BMP and WNT signaling sequentially (27) and discovered that the loss of *Stk40* increased the steady-state level of c-JUN proteins and impeded mesoderm differentiation. Moreover, STK40 could facilitate COP1–c-JUN complex formation to regulate c-JUN protein levels and ensure proper mesoderm differentiation. Taken together, the current study uncovers an important role and regulatory mechanism of STK40 in the control of mesoderm differentiation from pluripotent cells.

Results

Stk40 deletion impedes mesoderm differentiation

To test the hypothesis that the deletion of *Stk40* could impair mesoderm differentiation, we induced mESCs to differentiate toward the mesoderm lineage by modulating the activity of BMP4 and WNT signaling pathways sequentially, based on a previously published protocol (27). In brief, mESCs were cultured in N2B27 medium containing BMP4 (10 ng/ml) for 2 days followed by the addition of 1 μM CHIR99021 (CHIR) and 0.5% DMSO for 1 additional day (Fig. 1*A*). CHIR is used widely to activate WNT signaling by the inhibition of glycogen synthase kinase-3 (GSK3). To verify that ESCs were induced into the mesoderm lineage, expression levels of multiple marker genes in both WT and *Stk40*-null cells were examined at the indicated time points (Fig. 1, *B–E*). As expected, for pluripotency-associated genes, *Nanog* levels declined rapidly, whereas *Oct4* levels decreased gradually during differentiation. Expression of *Fgf5*, an epiblast marker, increased dramatically at differentiation days 1 and 2 but dropped to a relatively lower level at day 3. Notably, the mesoderm marker gene *T*, together with *Fgf8* and *Cdx2*, was substantially activated at differentiation day 3, suggesting that a mesoderm program was effectively induced (Fig. 1*B*). Moreover, the activation of WNT signaling was verified by elevated expression of *Rspo3*, an activator of the canonical WNT signaling pathway (28). Furthermore, immunofluorescence staining assays showed that the signal intensity of OCT4 and NANOG decreased along with the differentiation process (Fig. 1*D*), whereas the signal of T staining could only be detected at differentiation day 3 (Fig. 1*E*) rather than days 1 and 2 (data not show). Hence, the *in vitro* model of induced differentiation toward the mesoderm from ESCs was successfully established.

Comparison of marker gene expression levels between WT and *Stk40*-KO cells revealed that the lack of *Stk40* led to significant reductions of *Rspo3* as well as *T*, *Fgf8*, and *Cdx2* at differentiation day 3, without affecting expression profiles of *Oct4*, *Nanog*, and *Fgf5*, during ESC differentiation toward the mesoderm (Fig. 1, *B* and *C*). The finding suggested that STK40 might be required for the induction of the mesodermal program. Also, we found that mRNA and protein levels of STK40 increased moderately during the mesoderm differentiation process (Fig. 1, *B* and *C*), further supporting the notion that STK40 might contribute to mesoderm differentiation.

To further characterize the role of STK40 in mesoderm differentiation, immunofluorescence staining of T was conducted for cells at differentiation day 3. The signal intensity of T staining attenuated in *Stk40*-deleted cells (Fig. 1*E*). However, the expression of OCT4 and NANOG was not influenced upon *Stk40* ablation (Fig. 1*D*), suggesting that STK40 contributes to mesoderm differentiation without disturbing the pluripotency exit of ESCs. To quantify the efficiency of mesoderm differentiation, we established an mESC line stably expressing an shRNA sequence specifically targeting *Stk40* in the mESCs with the green fluorescence protein (GFP) targeted to the *Brachyury* locus (GFP-Bry ESCs) (29). The expression of the inserted GFP cassette is under the control of native *Brachyury* regulatory elements. Using the GFP-Bry ESC line, quantification of meso-

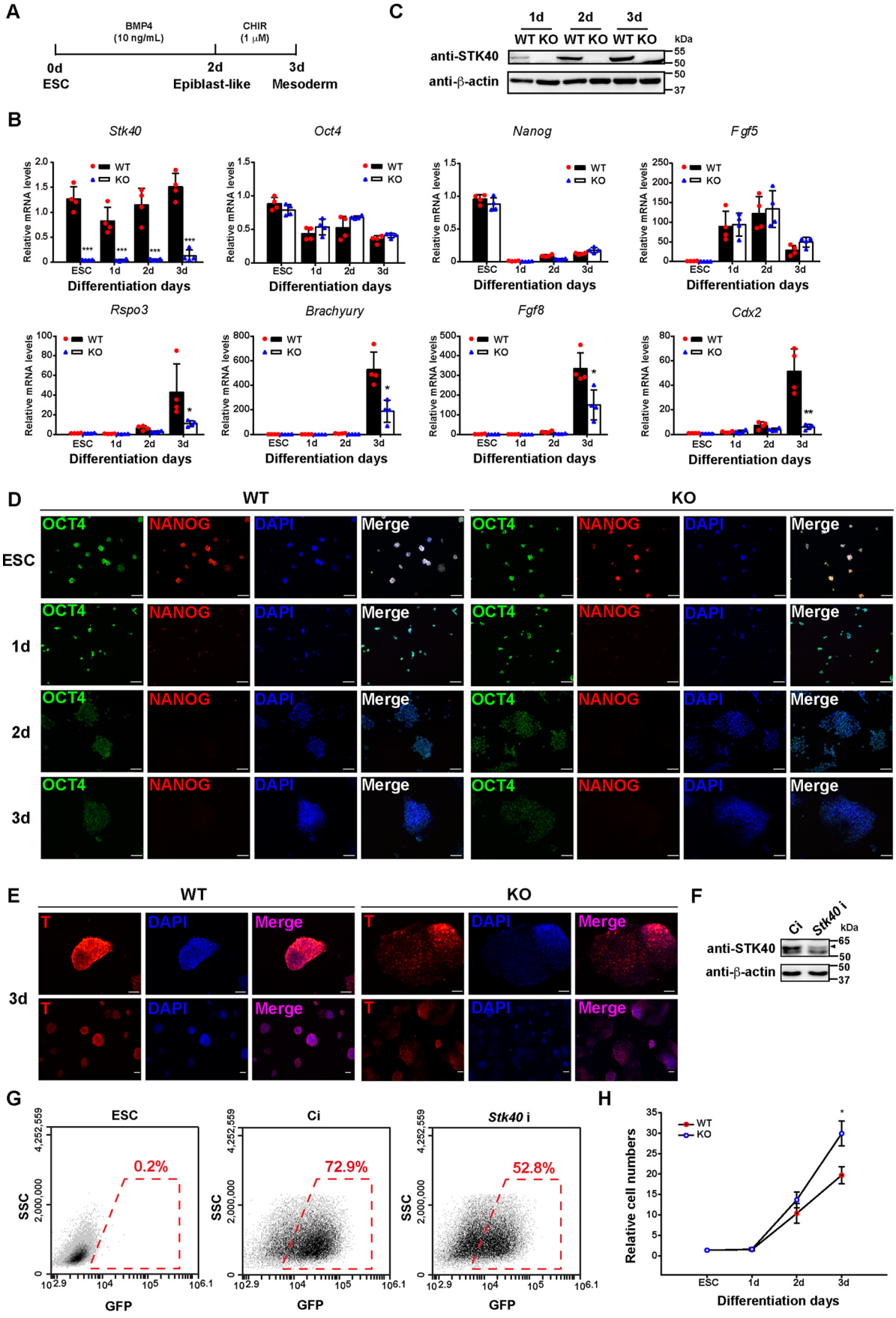
A
BMP4
(10 ng/mL)
CHIR
(1 μM)
0d
ESC
2d
Epiblast-like
3d
Mesoderm
C
1d
2d
3d
WT KO WT KO WT KO
kDa
anti-STK40
anti-β-actin
55
50
50
37
B
Stk40
Oct4
Nanog
Fgf5
Rspo3
Brachyury
Fgf8
Cdx2
WT
KO
Relative mRNA levels
Differentiation days
ESC
1d
2d
3d
D
WT
KO
ESC
1d
2d
3d
OCT4
NANOG
DAPI
Merge
E
WT
KO
3d
T
DAPI
Merge
F
Ci
Stk40 i
kDa
anti-STK40
anti-β-actin
65
50
50
37
G
ESC
Ci
Stk40 i
SSC
GFP
0.2%
72.9%
52.8%
4,252,559
2,000,000
0
10^2.9
10^4
10^5
10^6.1
H
WT
KO
Relative cell numbers
Differentiation days
ESC
1d
2d
3d

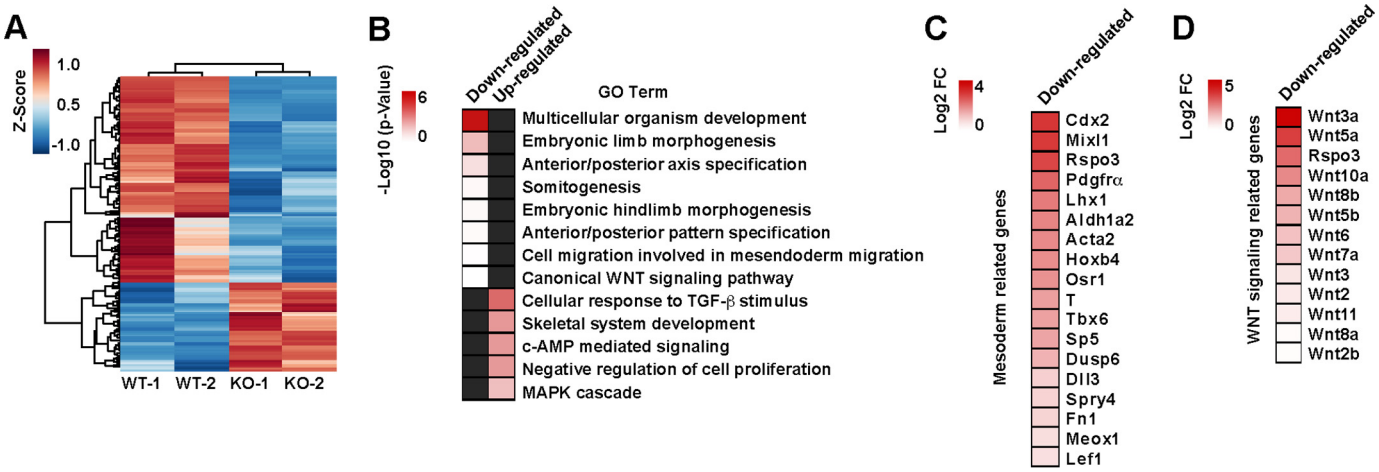

Figure 2. *Stk40* deletion attenuates the WNT signaling activity during mesoderm differentiation from ESCs. *A*, the heat map of differentially expressed genes between WT and *Stk40*-KO cells (p value <0.05) at mesoderm differentiation day 3 with two biological replicates of both WT and *Stk40*-KO cells. *B*, GO analyses of down-regulated and up-regulated genes, respectively, in *Stk40*-KO cells from the data sets of RNA-Seq in *A*. The DAVID method was applied to GO analyses, and enrichment levels of selected GO terms (p value <0.05) are marked by $-\log_{10}$ (p value). Missing values are shown as *black boxes*. *C* and *D*, the heat map of the mesoderm-related genes (*C*) and WNT signaling–related genes (*D*), which were down-regulated in *Stk40*-KO cells compared with WT cells at mesoderm differentiation day 3. -Fold change levels of selected genes are marked by $\log_2$ -fold change (*FC*) (p value <0.05). *TGF*, transforming growth factor; *MAPK*, mitogen-activated protein kinase.

derm induction becomes possible (30). We induced mesoderm differentiation from the GFP-Bry ESCs expressing either an *Stk40* shRNA or control shRNA and analyzed the GFP-positive cell population at differentiation day 3 by flow cytometry, taking the percentage of GFP-positive cells as an index of mesoderm differentiation efficiencies. Knockdown of *Stk40* was verified by Western blot analysis (Fig. 1*F*). About 72.9% GFP-positive cells were detected in the control group, whereas only 52.8% GFP-positive cells were found in cells expressing the *Stk40* shRNA (Fig. 1*G*), supporting the proposal that STK40 is required for the proper differentiation of mESCs into the mesoderm lineage. In addition, we compared the cell number between WT and *Stk40*-null cells during mesoderm differentiation and found that *Stk40* deletion led to a higher cell growth rate (Fig. 1*H*). These results indicate that the loss of *Stk40* impairs mesoderm differentiation from ESCs with a concomitant increase in the cell growth rate.

To gain a global view for roles of STK40 in mesoderm differentiation, we performed RNA-Seq for both WT and *Stk40*-KO cells at day 3 of mesoderm differentiation. Altogether, 25 up-regulated and 85 down-regulated genes were detected in *Stk40*-null cells compared with WT cells (Fig. 2*A*). Gene ontology (GO) analyses revealed that the down-regulated genes were enriched for terms like somitogenesis, mesendoderm migration, and canonical WNT signaling pathway (Fig. 2*B*), consistent with impaired mesoderm differentiation observed in *Stk40*-KO cells. Specifically, genes down-regulated upon *Stk40* ablation included an array of mesoderm-related genes, such as *T* and *Mixl1* (31) (Fig. 2*C*). Moreover, the expression of *Wnt3a*, *Wnt5a*, and *Rspo*3, known to exert important roles in mesodermal development through the WNT signaling pathway, was also attenuated in *Stk40*-deleted cells as compared with WT cells (Fig. 2*D*), implying that the reduced WNT signaling activity might, at least partially, account for the impaired mesoderm differentiation in *Stk40*-KO cells.

Stk40 deletion increases protein levels of c-JUN, repressing mesoderm differentiation

To explore how STK40 could be associated with the WNT signaling pathway, we employed mass spectrometric analysis to find proteins with distinct levels between the WT and *Stk40*-KO mouse embryonic fibroblasts (MEFs) (Fig. 3*A*). MEFs were chosen primarily due to their convenience in use as a cellular system. Interestingly, we found that AP-1 targets, such as DNMT1, CEBPβ, TGM2, FOSL2, APLS1, and JUNB (32), had higher protein amounts in *Stk40*-KO MEFs than in WT MEFs (Fig. 3*B*). AP-1 transcription factors, encompassing c-JUN, JUNB, JUND, c-FOS, and FRA-1, are known to control cellular proliferation, transformation, and death (8, 9, 33). Among AP-1 transcription factors, c-JUN plays critical roles in

Figure 1. *Stk40* deletion impairs mesoderm differentiation from ESCs. *A*, schematic illustration of the *in vitro* mesoderm differentiation procedure. *B*, qRT-PCR analysis of mRNA levels of marker genes at indicated time points during mesoderm differentiation from WT and *Stk40*-KO mESCs. Data were normalized to the expression of *Actb* and are represented as -fold changes relative to those in undifferentiated ESCs. *Error bars* denote the means ± S.D. (n = 4 independent experiments); Student's t test: *, $p < 0.05$; **, $p < 0.01$; ***, $p < 0.001$. *C*, representative Western blot analysis of STK40 protein levels during mesoderm differentiation. β-actin was used as a loading control. Data are representative of three independent experiments. The molecular mass (kDa) is given at the *right* side of the blot. *D*, representative results of immunofluorescence staining of OCT4 (*green*) and NANOG (*red*) in WT and *Stk40*-KO cells at the undifferentiated stage or differentiation days 1, 2, and 3. DAPI was used to label the nuclei (*blue*). *Scale bars* represent 50 μm. *E*, representative results of immunofluorescence staining of T (*red*) in WT and *Stk40*-KO cells at differentiation day 3. One colony is presented in the *upper panel*, and the *lower panel* shows colonies at the lower magnification. DAPI was used to label the nuclei (*blue*). *Scale bars* represent 50 μm. Similar results were obtained in at least three independent experiments. *F*, the knockdown efficiency of a transduced *Stk40* shRNA was evaluated by the Western blot analysis at differentiation day 3. β-actin was used as a loading control. The *arrowhead* indicates the specific signal of STK40. *G*, representative flow cytometric analysis for the percentage of T-positive cells at mesoderm differentiation day 3 from control shRNA (*Ci*)– and *Stk40* shRNA (*Stk40 i*)–transduced GFP-Bry ESCs. Undifferentiated ESCs were used as a control. Similar results were obtained from four independent experiments. *H*, quantification of relative cell numbers during mesoderm differentiation from WT and *Stk40*-KO ESCs. *Error bars* denote the means ± S.D. (n = 3); Student's t test: *, $p < 0.05$. *d*, days.

a broad range of developmental events in a dosage-dependent manner (33), and it was previously reported to participate in the modulation of canonical WNT signaling (12). Hence, we tested whether there was a difference in the c-JUN protein levels between WT and *Stk40*-KO MEFs. Indeed, the c-JUN protein level was obviously higher in *Stk40*-KO MEFs than in WT cells (Fig. 3*C*). To learn whether the c-JUN protein level would also be higher in *Stk40*-KO cells during mesoderm differentiation of ESCs, we measured both phosphorylated (Ser-63/Ser-73) and total c-JUN protein levels at 3, 6, 12, and 24 h post-CHIR addition after differentiation for 2 days. Consistently, higher total c-JUN protein levels were detected in *Stk40*-KO cells than in WT cells at all time points tested (Fig. 3*D*), although *Stk40* KO did not alter the transcript level of c-*Jun* (Fig. 3*F*). In addition, the levels of phosphorylated c-JUN at serine residues 63 and 73 were also higher in *Stk40*-KO cells than in WT cells at most time points examined. However, there was not a discerned difference in protein levels of phosphorylated c-JUN N-terminal

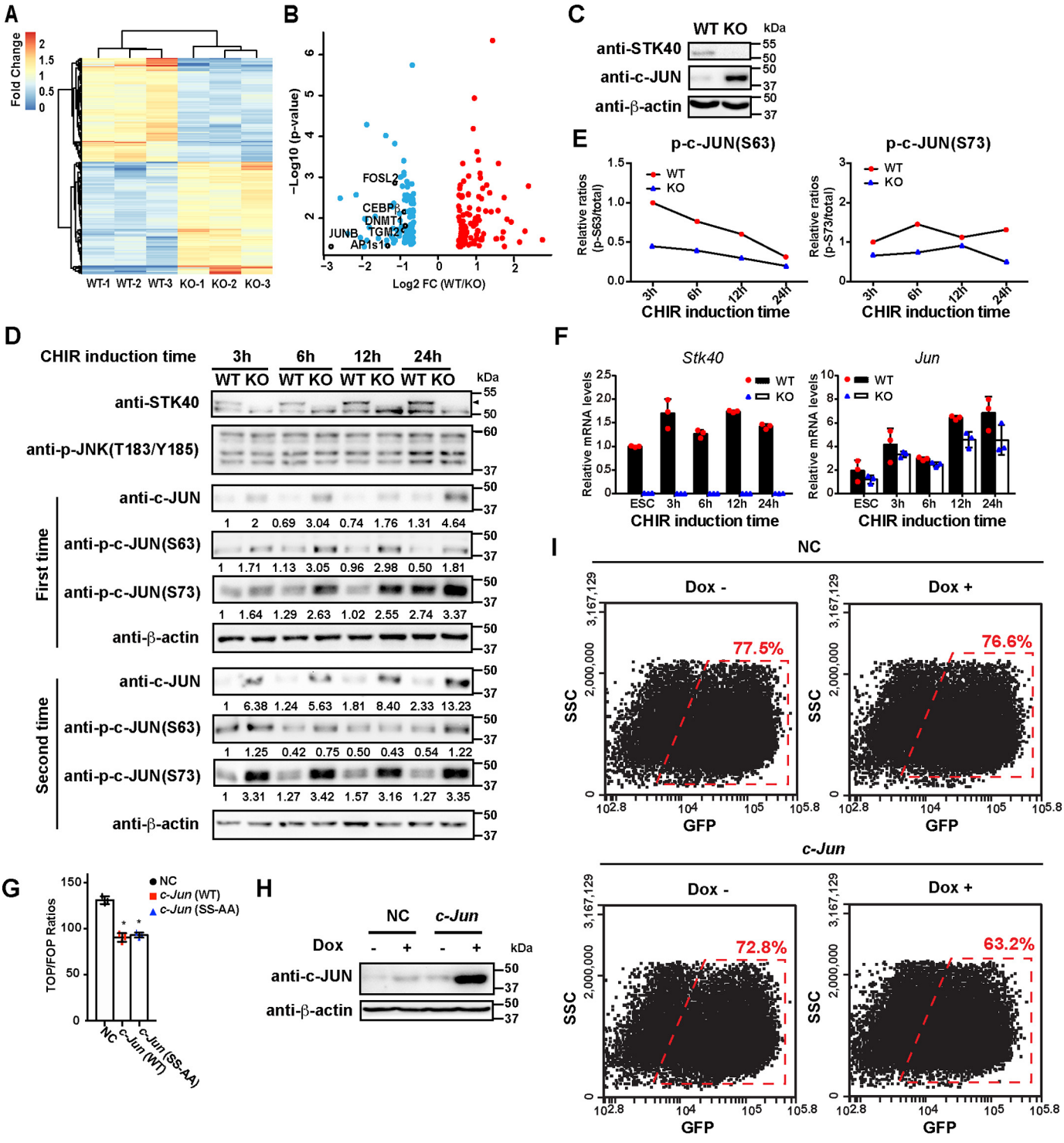

kinases (JNKs) (Fig. 3*D*), which have been reported to phosphorylate c-JUN within its N terminus (34). Despite simultaneous increases in both total and phosphorylated c-JUN protein amounts, ratios of phosphorylated c-JUN/total c-JUN proteins for their relative levels at different time points decreased in *Stk40*-KO cells for both Ser-63 and Ser-73 phosphorylation as compared with that in WT cells post-CHIR treatment (Fig. 3*E*). These results indicate that STK40 could modulate the level of c-JUN proteins at a posttranscriptional level.

Given that WNT signaling was enriched in genes down-regulated by *Stk40* KO (Fig. 2*B*) and that c-JUN was reported to participate in the regulation of WNT signaling (12), we conducted the TOP/FOPFlash luciferase reporter assay to determine the role of c-JUN in controlling WNT signaling activity and found that overexpression of c-JUN or its phospho-dead (SS-AA; the mutation from serine to alanine at residues Ser-63/Ser-73) mutant in 293FT cells reduced WNT signaling activity in the presence of CHIR (Fig. 3*G*), suggesting that ectopic expression of c-*Jun* could suppress the WNT signaling activity independently of c-JUN phosphorylation at Ser-63/Ser-73.

The aforementioned findings implied that STK40 might modulate WNT signaling activities through controlling c-JUN protein levels during mesoderm differentiation. To address this issue, we established a doxycycline (Dox)-induced c-*Jun* overexpression system in the GFP-Bry ESCs. Addition of Dox induced overexpression of c-JUN in c-*Jun* sequence– containing virus-infected cells but not in empty vector virus–infected cells (Fig. 3*H*). At differentiation day 3, the proportion of GFP-positive cells was lower in cells overexpressing exogenous c-*Jun* as compared with that in cells without exogenous c-*Jun* (Fig. 3*I*). Therefore, our results indicate that an abnormally high level of c-JUN has a suppressive effect on mesoderm differentiation from ESCs.

STK40 interacts with c-JUN and facilitates the formation of c-JUN and COP1 protein complexes

It is known that c-JUN proteins can be degraded through the UPS by several E3 ligases, such as COP1 (35), MEKK1 (36), FBW7 (37), and ITCH (38). Of note, STK40 was recently reported to bind to COP1 directly, possibly serving as a COP1 adaptor to recruit substrates (26). Hence, we anticipated that STK40 might control the c-JUN protein level by modulating the interaction between COP1 and c-JUN to promote c-JUN degradation. To test this hypothesis, we first validated the interaction between STK40 and COP1 as well as between STK40 and c-JUN by GST pulldown and coimmunoprecipitation (co-IP) assays, respectively. GST-STK40 specifically bound to His-c-JUN and His-COP1 *in vitro*, respectively (Fig. 4*A*). As a negative control, GST alone was not able to associate with either His-c-JUN or His-COP1. We next examined which region(s) of STK40 was responsible for its interaction with c-JUN or COP1. To this end, we generated FLAG-tagged expression vectors containing the coding sequences for the three truncated forms of STK40: the lack of the N terminus (ΔN), the lack of C terminus (ΔC), and the kinase homolog domain (PK) (Fig. 4*B*). Then, HA-tagged c-*Jun* expression vectors were cotransfected into 293FT cells in combination with FLAG-tagged WT or truncated *Stk40* expression vectors. The lack of the C terminus on STK40 abrogated its interaction with c-JUN, whereas the absence of the N terminus augmented the association between STK40 and c-JUN (Fig. 4*C*). This observation suggested that the C terminus of STK40 was required for its interaction with c-JUN, whereas the N-terminal region might have a negative impact on the interaction between STK40 and c-JUN. Similarly, the interaction between STK40 and COP1 was abrogated by the deletion of the C-terminal region. However, their interaction was not affected by the absence of the N-terminal region of STK40 (Fig. 4*D*).

Posttranslational modifications could regulate protein interactions, and phosphorylation is perhaps one of the most studied modifications with respect to modulating binding affinity of proteins. To learn how the N-terminal region of STK40 affected its interaction with c-JUN, we examined phosphorylation sites within this region through prediction using the web tool DISPHOS (www.dabi.temple.edu/disphos) (39).[4] Among the four predicted residues, the serine at residue 6 (Ser-6) had the highest scores (Fig. 4*E*). Hence, we investigated whether STK40 mutants of phospho-dead (S6A, the mutation from serine to alanine) and phosphomimic (S6E, the mutation from serine to glutamic acid) could impact the interaction between STK40 and c-JUN by co-IP assays. We found that the S6A STK40 mutant displayed an obviously stronger association with c-JUN than did WT STK40. In contrast, the S6E STK40 mutant had a

[4] Please note that the JBC is not responsible for the long-term archiving and maintenance of this site or any other third party hosted site.

Figure 3. *Stk40* knockout increases c-JUN protein levels in MEFs and during mesoderm differentiation. *A*, the heat map showing differences in protein levels between WT and *Stk40*-KO MEFs (p value <0.05) identified by mass spectrometric analysis, with three biological replicates for each cell type. *B*, a volcano plot representing the increased (*blue*) and decreased (*red*) proteins in *Stk40*-KO MEFs as compared with WT MEFs, based on data sets from *A*. AP-1 family–related proteins are marked with *black circles* in the plot. *C*, a representative Western blot analysis for protein levels of STK40 and c-JUN in WT and *Stk40*-KO MEFs. β-actin was used as a loading control. *D*, at the indicated time points of CHIR treatment after mesoderm differentiation for 2 days from WT and *Stk40*-KO ESCs, protein levels of STK40, JNK (p-Thr-183/Tyr-185), c-JUN, c-JUN (p-Ser-63), and c-JUN (p-Ser-73) were analyzed by Western blotting. Results for analyses of c-JUN and phosphorylated c-JUN levels from two independent experiments are shown. *E*, the *gray* values of phosphorylated c-JUN and total c-JUN in *D* were quantified using ImageJ software, and the relative protein levels were calculated by comparing the *gray* values from the indicated time points with that from WT cells at 3 h after CHIR induction. Then, ratios of phosphorylated c-JUN/total c-JUN proteins were obtained by comparing the values of relative protein levels. The mean values of ratios (p-Ser-63 c-JUN or p-Ser-73 c-JUN)/total c-JUN) from the two independent experiments were calculated and are presented in the plots. *F*, relative mRNA levels of *Stk40* and *Jun* (c-JUN) were measured by qRT-PCR. Data were normalized to the level of *Actb* and are represented as -fold changes (*FC*) relative to those in undifferentiated ESCs. *Error bars* denote the means ± S.D. ($n = 3$); Student's t test: ***, $p < 0.001$. *G*, TOP/FOPFlash assays showing that overexpression of the WT or SS-AA mutant c-*Jun* attenuates the WNT signaling activity in 293FT cells. The TOPFlash or FOPFlash plasmid plus c-*Jun*, c-*Jun*(SS-AA), or an empty vector was transfected into 293FT cells, and cells were treated with CHIR at 1 μM for 6 h prior to sample collection. Luciferase activity ratios were determined by (TOP firefly/*Renilla*)/(FOP firefly/*Renilla*). *H*, representative Western blot analysis of Dox-induced c-*Jun* overexpression at mesoderm differentiation day 3 from GFP-Bry ESCs. β-actin was used as a loading control. *I*, representative flow cytometric analysis of GFP-positive cells at differentiation day 3 with or without c-*Jun* overexpression. Similar results were obtained in two independent experiments. *NC*, an empty vector; *SSC*, side scatter.

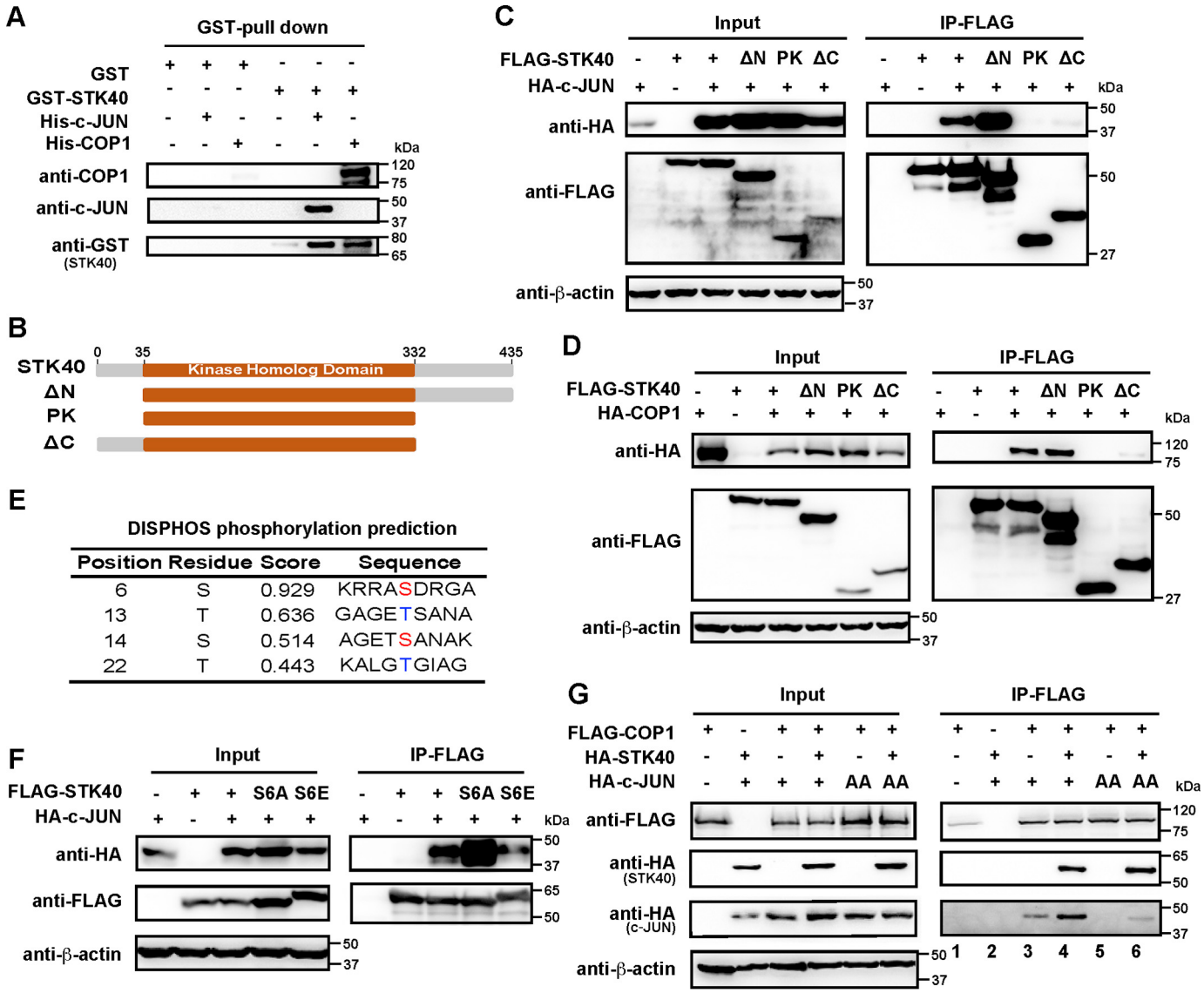

Figure 4. STK40 facilitates the association between c-JUN and COP1. *A*, representative Western blot analysis of GST-STK40 pulldown assays. GST or GST-STK40 fusion proteins were incubated with His-c-JUN or His-COP1 fusion proteins and precipitated by GSH-Sepharose 4B beads. Precipitated His-c-JUN or His-COP1 proteins were visualized by Western blotting. Similar results were obtained from at least three independent experiments. *B*, a schematic representation of the modular architecture of WT and truncated STK40. *C* and *D*, representative Western blot analysis of interactions between WT or truncated STK40 and c-JUN (*C*) or COP1 (*D*). WT or truncated *Stk40* expression vectors were transfected into 293FT cells in combination with *HA-c-Jun* or *HA-Cop1* plasmids. Whole-cell lysates were immunoprecipitated with anti-FLAG M2 beads and analyzed by Western blotting with anti-HA or anti-FLAG antibodies (*right panel*). The expression of FLAG-tagged STK40, HA-tagged c-JUN, and HA-tagged COP1 was verified by immunoblotting with anti-FLAG and anti-HA antibodies, respectively (*left panel*). Data are representative of three independent experiments. *E*, phosphorylation sites at the N-terminal domain of STK40 were predicted by DISPHOS (39) (www.dabi.temple.edu/disphos).[4] *F*, the STK40 mutants of phospho-dead (S6A) and phosphomimic (S6E) impact the interaction between STK40 and c-JUN. WT or mutated *Stk40* expression vectors were cotransfected with c-*Jun* constructs into 293FT cells. Whole-cell lysates were immunoprecipitated with anti-FLAG M2 beads and analyzed by Western blotting with anti-HA or anti-FLAG antibodies (*right panel*). S6A denotes the mutation from serine (S) to alanine (A), and S6E denotes the mutation from serine to glutamic acid (E) at serine residue 6. Data are representative of three independent experiments. *G*, STK40 could mediate the interaction between c-JUN and COP1. The FLAG–COP1 protein complexes were immunoprecipitated from 293FT cells with anti-FLAG M2 beads and analyzed by Western blotting with the antibodies indicated. β-actin was used as a loading control. AA denotes the mutation from ^{235}VP^{236} to AA. Data are representative of three independent experiments.

weaker interaction with c-JUN compared with WT STK40 (Fig. 4*F*). The result suggests that the phosphorylation of the N-terminal Ser-6 could interfere with the interaction between STK40 and c-JUN.

To address the question of whether STK40 could modulate the formation of COP1 and c-JUN complexes to control the c-JUN protein level, co-IP assays were conducted to determine the binding intensity between COP1 and c-JUN in the presence and absence of exogenous STK40, respectively. Overexpression of HA-tagged *Stk40* enhanced the interaction between COP1 and c-JUN in 293FT cells (Fig. 4*G*, *right panel*, *lane 4 versus lane 3*). COP1 was previously shown to bind the VP motif of c-JUN, and a mutation of VP to AA disrupted the direct interaction between COP1 and c-JUN (16, 35). Consistently, our co-IP assay results showed that c-JUN(AA) could not interact with COP1 (Fig. 4*G*, *right panel*, *lane 5*). Interestingly, in the presence of exogenous STK40, a relatively weak interaction between COP1 and c-JUN(AA) was detected (Fig. 4*G*, *right*

panel, *lane 6*). Therefore, we propose that STK40 could enhance the interaction between COP1 and c-JUN.

STK40 promotes c-JUN protein degradation partially through COP1

Considering that *Stk40* ablation led to elevated levels of c-JUN proteins and that STK40 facilitated the interaction between COP1 and c-JUN, we predicted that STK40 might accelerate c-JUN protein degradation. To test this idea, we blocked protein synthesis by cycloheximide (CHX) treatment to analyze c-JUN protein stability in WT and *Stk40*-KO MEFs. As expected, the protein stability of c-JUN was higher in *Stk40*-KO MEFs than in WT MEFs (Fig. 5*A*). Consistently, the reintroduction of *Stk40* into *Stk40*-KO MEFs reduced steady-state levels of c-JUN protein in a *Stk40* dosage–dependent manner (Fig. 5*B*). In contrast, the stability and amount of COP1 proteins were not affected by *Stk40* expression levels (Fig. 5, *A* and *B*). These results suggest that STK40 participates in the control of c-JUN protein stability.

To gain experimental evidence that COP1 is involved in STK40-mediated control of c-JUN protein levels, we silenced the expression of *Cop1* in MEFs using an shRNA interference approach. Western blotting results showed that knockdown of *Cop1* increased c-JUN protein levels in both WT and *Stk40*-KO MEFs and that the c-JUN protein level was highest in *Stk40*-KO cells expressing the *Cop1* shRNA, although there was a lower -fold change in c-JUN protein levels between *Cop1*-knockdown and control MEFs in the absence of *Stk40* (Fig. 5*C*, *lane 6 versus lane 2*) than that in the presence of *Stk40* (Fig. 5*C*, *lane 5 versus lane 1*). Of note, overexpression of *Stk40-GFP* fusion proteins decreased the amount of c-JUN proteins in *Stk40*-KO MEFs (Fig. 5*C*, *lane 4 versus lane 2*). However, the rescue effect of *Stk40* overexpression was attenuated when *Cop1* was silenced (Fig. 5*C*, *lane 8 versus lane 6* and *lane 8 versus lane 4*), suggesting that STK40-mediated control of c-JUN protein level is, at least partially, dependent on COP1.

To determine the role of COP1 in the control of c-JUN protein amounts and mesoderm differentiation from ESCs, we silenced *Cop1* expression by two sets of shRNAs specifically targeting *Cop1*, respectively, in the GFP-Bry ESCs, which were induced to mesoderm differentiation as described in Fig. 1*A*. At day 3 of differentiation, GFP-positive cells were analyzed by flow cytometry. The high efficiency of *Cop1* knockdown was validated by Western blot analysis. Cells expressing *Cop1* shRNAs had markedly higher c-JUN protein levels than control cells (Fig. 5*D*). Compared with cells expressing the control shRNA, the percentage of GFP-positive cells decreased dramatically in cells expressing *Cop1* shRNAs (Fig. 5*E*). Therefore, COP1 plays an important role in tightly controlling c-JUN protein levels during mesoderm differentiation.

Stk40 deletion impairs mesoderm differentiation and leads to c-JUN protein accumulation in vivo

To determine whether STK40 participates in mesoderm development *in vivo*, we conducted whole-mount immunofluorescence staining of mouse embryos at the gastrulation stage (E7.0) when T-positive cells migrate from the posterior to anterior region to establish mesodermal and endodermal layers (30, 40). Antibodies against T and SOX2 were employed for the whole-mount staining to mark the mesodermal and ectodermal cells, respectively. Altogether, 10 WT and 17 *Stk40*-null embryos were subjected to immunostaining assays. Confocal imaging analyses demonstrated that T-positive cells distributed similarly in WT and *Stk40* KO embryos, but the signal intensity of T was drastically reduced in *Stk40*-KO embryos. Statistically, eight of 10 WT and five of 17 *Stk40*-KO embryos displayed normal T signal intensities, whereas two of 10 WT and 12 of 17 *Stk40*-null embryos showed weak T signals. These observations suggest that STK40 is required for the proper differentiation of pluripotent cells into T-positive cells at the gastrulation stage. As a control, *Stk40* ablation did not affect signal intensities of SOX2 staining significantly (Fig. 6*A*).

Due to the ubiquitous function of c-JUN in many cell types, we posited that STK40 might modulate c-JUN protein levels in a variety of tissues. We compared c-JUN protein levels in the limb, liver, and head between WT and *Stk40*-KO embryos at E13.5 and found that c-JUN protein levels were higher in the limb, liver, and head from *Stk40*-KO embryos than in WT counterparts, whereas there was no difference in the level of COP1 proteins in the limb, liver, and head between WT and *Stk40*-KO embryos (Fig. 6*B*). Therefore, STK40 might control the c-JUN protein level in multiple organs/tissues of mouse embryos.

Discussion

c-JUN is expressed in a wide range of cell types in developmental processes and is essential for normal mouse development (41). Moreover, high c-JUN abundance shows a tight correlation with the tumorigenesis of several cell lines (9, 42). Thus, it is of significance to address the question of how c-JUN levels are modulated. Here, we report that STK40 could be an important new regulator of c-JUN protein amount. Additionally, our study reveals that STK40 might control c-JUN protein turnover through modulating the formation of COP1 and c-JUN complexes. Functionally, we show that this STK40–COP1–c-JUN axis plays a role in mesoderm differentiation (Fig. 7).

Our previous studies showed that *Stk40* ablation in mice leads to developmental disorders in multiple mesoderm-derived cell types (22–25). Thus, we speculated that STK40 might be involved in mesoderm development. Utilizing an *in vitro* model of mesoderm induction from mESCs, we explored the function of *Stk40* in mesoderm differentiation at both the molecular and cellular levels. By analyzing the RNA-Seq data from WT and *Stk40*-KO cells at mesoderm differentiation day 3, we found that expression levels of some WNT family members were lower in *Stk40*-ablated cells than in WT cells, and some of these WNT family members are known to play critical roles in mesoderm development (4, 6, 43). Therefore, attenuated WNT signaling might be responsible for the impaired mesoderm differentiation caused by *Stk40* KO. c-JUN has previously been reported to bridge TCF and Dvl, and its N-terminal phosphorylation is likely required in the canonical WNT signaling pathway. Functionally, c-JUN contributes to the induction of ventral mesoderm in zebrafish (12). In this study, we revealed that both phosphorylated and total c-JUN protein

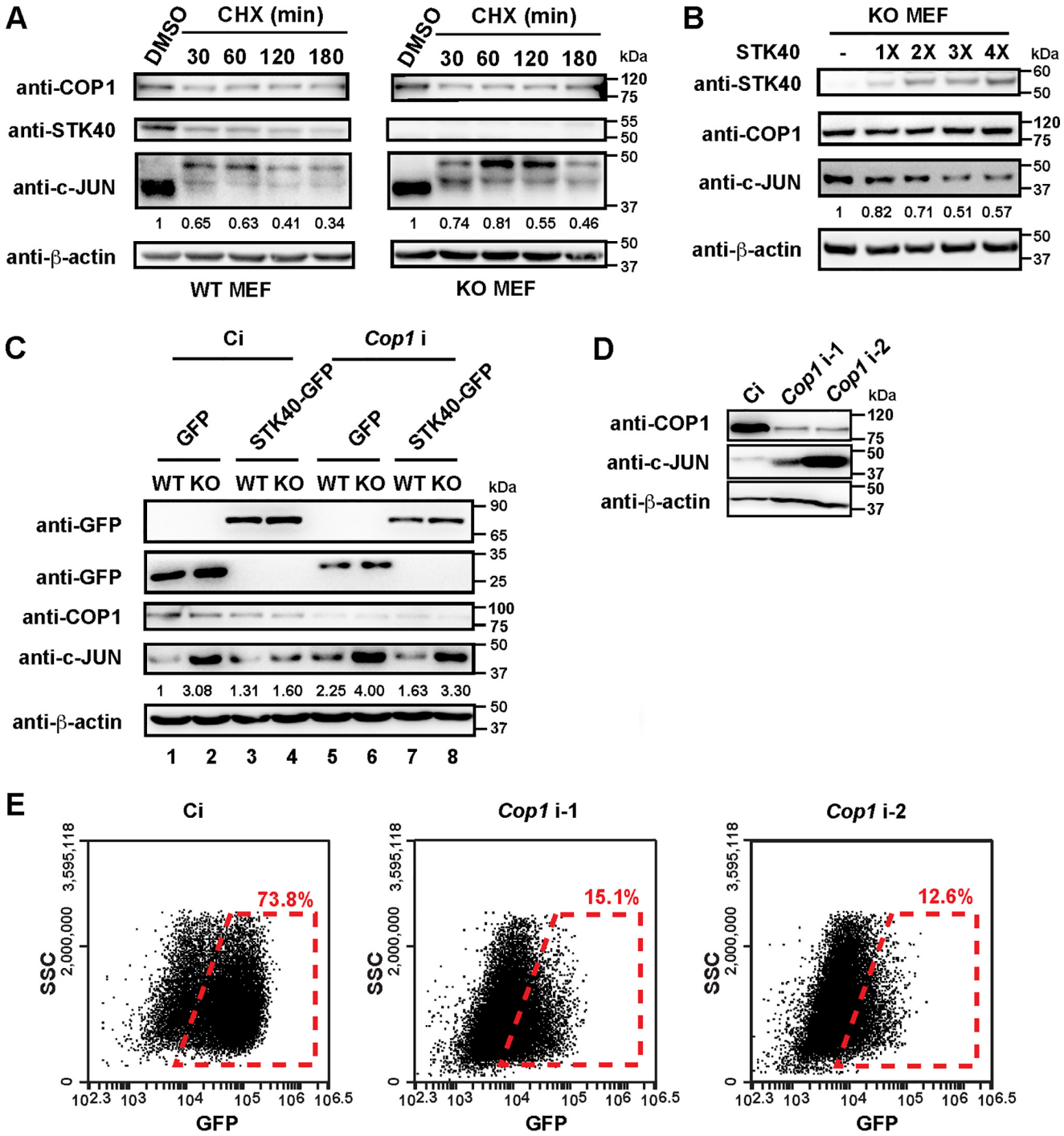

Figure 5. STK40 promotes c-JUN protein turnover partially depending on COP1. *A*, protein stability of COP1, STK40, and c-JUN was evaluated by Western blot analysis. Prior to sample collection, WT and *Stk40*-KO MEFs were treated with either 50 μM CHX for the indicated length of time or DMSO for 180 min. The total cell lysate was extracted and subjected to Western blot analysis. The *gray* density of the c-JUN blot was measured by ImageJ software and is indicated. *B*, representative Western blot analysis of c-JUN, STK40, and COP1 protein levels in *Stk40*-KO MEFs with or without overexpression of *Stk40* at different dosages after viral infection for 48 h. *C*, STK40-mediated attenuation of c-JUN protein level is partially dependent on COP1. Viral shRNAs of control (*Ci*) or *Cop1* (a mixture of *Cop1* i-1 and *Cop1* i-2 shRNAs) together with viral *GFP* or *Stk40-GFP* were delivered in WT and *Stk40*-KO MEFs, respectively. Protein levels of GFP, STK40-GFP, COP1, and c-JUN were analyzed by Western blotting at 48 h postinfection. β-actin was used as a loading control. *D*, viral shRNAs of control (*Ci*), *Cop1* i-1, or *Cop1* i-2 were delivered in GFP-Bry ESCs. The expression levels of COP1 and c-JUN were analyzed by Western blotting. *E*, a representative result for percentages of GFP-positive cells from control and *Cop1*-knockdown cells analyzed by flow cytometry at day 3 of mesoderm differentiation from GFP-Bry ESCs. *SSC*, side scatter.

levels were elevated upon *Stk40* ablation. However, ratios of the phosphorylated (Ser-63 or Ser-73)/total c-JUN levels were lower in *Stk40* KO cells than in WT cells during mesoderm differentiation from ESCs, providing a possible explanation for the reduced WNT signaling activity in *Stk40*-deleted cells. Moreover, overexpression of c-*Jun* suppressed WNT signaling activity and decreased the percentage of T-positive mesoderm-like cell populations at day 3 of ESC differentiation. In line with

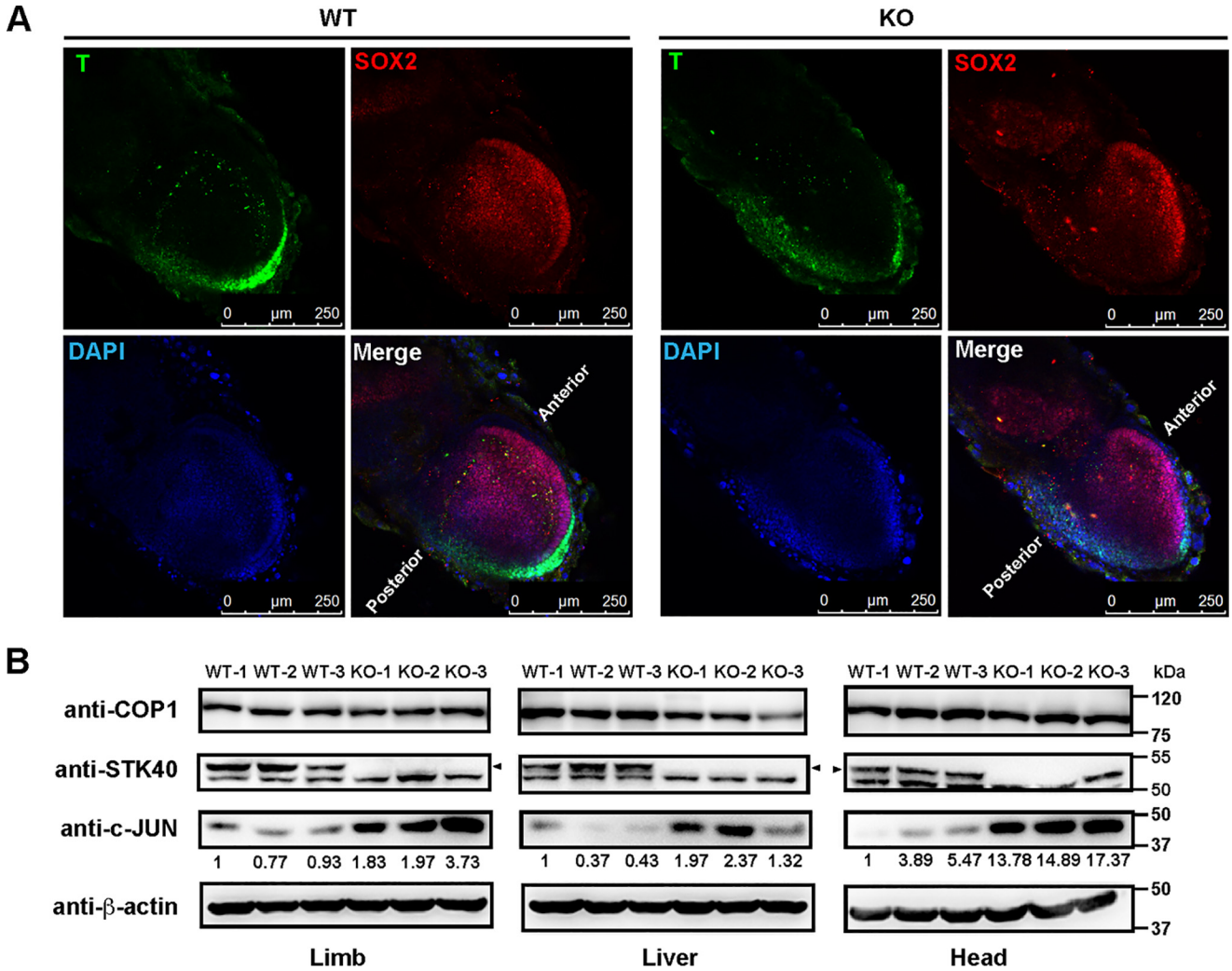

Figure 6. *Stk40* deletion impairs mesoderm development and enhances c-JUN abundance *in vivo*. *A*, representative whole-mount immunofluorescence staining images of T (*green*) and SOX2 (*red*) in WT and *Stk40*-KO embryos at E7.0. A normal T–staining image in a WT embryo and a weak T–staining image in a *Stk40*-KO embryo are shown. DAPI was used to label the nuclei (*blue*). *Scale bars* represent 250 μm. *B*, protein levels of COP1, STK40, and c-JUN in the limb, liver, and head of WT and *Stk40*-KO embryos at E13.5 were analyzed by Western blotting. The *arrowhead* indicates the specific signal of STK40. β-actin was used as a loading control. Samples were collected from three WT (WT-1, WT-2, and WT-3) and three *Stk40*-KO embryos (KO-1, KO-2, and KO-3), respectively.

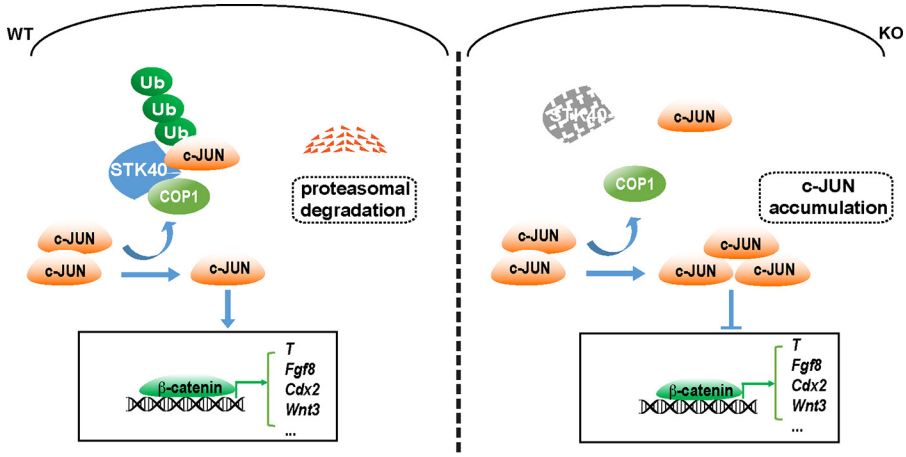

Figure 7. The schematic illustration of how STK40 contributes to mesoderm induction from mESCs. STK40 facilitates the association between COP1 and c-JUN, likely leading to proteasomal degradation of c-JUN, and the proper amount of c-JUN ensures mesoderm differentiation. In the absence of *Stk40*, mesoderm induction from mESCs is impaired at least partially due to c-JUN protein accumulation and WNT signaling inhibition. *Ub*, ubiquitin.

our finding, Liu *et al.* (11) reported that overexpression of c-*Jun* in mESCs leads to the activation of certain endodermal marker genes with the concomitant repression of *T*. Collectively, we propose that the appropriate level of c-JUN, especially its phosphorylation state, participates in the control of mesoderm differentiation, probably through modulating the WNT signaling pathway.

COP1 was previously shown to recruit c-JUN to a multisubunit ubiquitin ligase complex containing DNA damage–binding protein-1 (DDB1), Cullin 4A, and regulator of Cullins-1 (ROC1) rather than acting as an E3 ligase to catalyze c-JUN ubiquitination directly (16). Here, we unveiled that overexpression of *Stk40* enhanced the interaction between COP1 and c-JUN. The mutation of the VP motif of c-JUN abrogated the interaction between COP1 and c-JUN(AA). However, in the presence of exogenous STK40, the interaction between COP1 and c-JUN(AA) could be detected. Subsequently, c-JUN might be ubiquitinated by the multisubunit ubiquitin ligase complex (DET1–DDB1–Cullin 4A–RBX1) and degraded through the UPS. Moreover, we found one component of the ubiquitin ligase complex, DET1, in proteins potentially interacting with STK40 from a public database (BioPlex 2.0 data set) (44), supporting the possibility that STK40 might recruit the ubiquitin ligase complex to down-regulate c-JUN protein levels. Nevertheless, we could not exclude the possibility that COP1 might serve as an E3 ligase to add ubiquitin molecules on c-JUN directly in our context. More studies should be conducted to address the question of how STK40 precisely modulates c-JUN protein stability through COP1.

Taken together, our study suggests that STK40 promotes COP1 and c-JUN to form complexes, hence maintaining c-JUN proteins at an appropriate level and taking part in the regulation of mesoderm development (Fig. 7). The molecular mechanism described here not only extends our understanding of how COP1 regulates c-JUN protein stability but also uncovers STK40 and COP1 as new regulators for mesoderm differentiation. Additionally, given the well-established roles of c-JUN in cancers, our finding may provide potential therapeutic targets to treat diseases.

Experimental procedures

Animals

Animals were raised under the condition described previously and performed according to the guidelines approved by the Shanghai Jiao Tong University School of Medicine (22). The genotype of WT (*Stk40*$^{+/+}$) and *Stk40*-KO (*Stk40*$^{-/-}$) mice was determined as described previously (22).

Cell culture and differentiation

mESCs were derived from WT and *Stk40*-KO blastocysts (22) as described previously (45). The ESCs were maintained on inactivated MEF feeders in N2B27 medium with 2 mM GlutaMAX (Gibco), 0.1 mM nonessential amino acids, 0.1 mM β-mercaptoethanol (Sigma), 1000 units/ml leukemia inhibitory factor (Millipore), 3 μM CHIR99021, and 1 μM PD0325901 (STEMCELL Technologies) (46). Cell colonies were digested into single cells for regular passaging using Accutase (STEMCELL Technologies). For induced mesoderm differentiation from mESCs, cells were passaged onto gelatin-coated cell culture plates to remove feeder cells prior to the initiation of differentiation. After one passage, ESCs were dissociated with Accutase, and 1.5×10^5 cells were seeded in 1 well of 6-well plates precoated with gelatin and maintained in N2B27 medium with addition of 1% KnockOut Serum Replacement (Gibco), 0.1% BSA (Gibco), and 10 ng/ml BMP4 (R&D Systems) for 2 days. Then, the medium was replaced by a DMEM-based medium with 15% KnockOut Serum Replacement, 1 μM CHIR99021 (STEMCELL Technologies), and 0.5% DMSO (Sigma) for 1 additional day (27).

MEFs were generated from E13.5 mouse embryos and cultured in medium consisting of DMEM (Gibco) supplemented with 10% fetal bovine serum (Gibco). Plat-E (Cell Biolabs) and 293FT (Invitrogen) cell lines were cultured in 293FT medium consisting of DMEM (Gibco) supplemented with 10% fetal bovine serum (Gibco), 2 mM GlutaMAX (Gibco), 1 mM pyruvate sodium (Gibco), and 0.1 mM nonessential amino acid (Gibco).

Virus preparation

For *Stk40* and *Cop1* knockdown assays, the DNA encoding sequences of shRNA specific to *Stk40* and *Cop1* were cloned into the pLKO.1 plasmid, respectively. Sense sequences for *Stk40*, *Cop1*, and control RNAi were as follows: *Stk40* shRNA-1, 5′-GGACCCATCGGATAACTAT-3′; *Stk40* shRNA-2, 5′-TGCATACCGAGTACTCTCT-3′; *Cop1* shRNA-1, 5′-CCTTGGTATAACAGCACATTA-3′; *Cop1* shRNA-2, 5′-GACAAATGGGCATGGCTAGAA-3′; control shRNA, 5′-GTGCGCTGCTGGTGCCAAC-3′.

For overexpression assays, cDNA sequences of *Stk40* or *Stk40-GFP* were inserted into pMXs plasmid. For inducible overexpression assays, the cDNA sequence of c-*Jun* was inserted into the pLVX-Tight-puro vector, and the Tet-On advanced inducible gene expression system was established according to the manufacturer's user manual (Clontech). Viral packaging and transduction were performed as described previously (24).

RNA extraction, cDNA synthesis, and quantitative real-time PCR (qRT-PCR)

Total RNA was extracted using TRIzol reagent (Invitrogen) and reverse transcribed into cDNA utilizing oligo(dT)$_{18}$ and ReverTra Ace reverse transcriptase (Toyobo). qRT-PCR was performed using the ABI PRISM 7900 Fast Real-Time PCR system (Applied Biosystems) and SYBR Premix Ex Taq (Takara). The primer sequences for qRT-PCR are provided in Table S1.

RNA-Seq

Total RNA was extracted from WT and *Stk40*-0KO cells collected at mesoderm differentiation day 3 using TRIzol reagent. Sequencing libraries were prepared according to Illumina's instructions. Paired-end RNA-Seq of 2×150-bp reads were sequenced on the Illumina HiSeq X Ten. Salmon software was used to calculate the samples' transcripts per million and raw counts (47). DESeq2 (48) was then used to identify differentially expressed genes with the following setting: adjusted p value <0.05. RNA-Seq raw data were submitted to

GEO (accession number GSE125877), and processed data are provided in Table S2.

Protein extraction and Western blot analysis

Total protein extracted from cells or mouse tissues was prepared with radioimmune precipitation assay lysis buffer (1 mM EDTA, 1% Nonidet P-40, 50 mM Tris (pH 7.5), 150 mM NaCl, and 10% glycerol), and protein concentrations were determined using the Pierce BCA Protein Assay kit (Thermo Fisher) following the manufacturer's instructions. Proteins were separated by SDS-PAGE and transferred to nitrocellulose membranes (GE Healthcare). Membranes were incubated with specific primary antibodies, and the antibody–protein complexes were visualized by horseradish peroxidase–conjugated secondary antibodies (Jackson ImmunoResearch Laboratories) and Pierce ECL Western Blotting Substrate (Thermo Fisher). Primary antibodies used for Western blotting are provided in Table S3.

Mass spectrometry

The mass spectrometric analysis was performed as described previously (49).

Digestion and TMT labeling—WT and *Stk40*-KO MEF samples were lysed using urea lysis buffer (8 M urea, 75 mM NaCl, 50 mM Tris (pH 8.2), 1% (v/v) EDTA-free protease inhibitor, 1 mM NaF, 1 mM β-glycerophosphate, 1 mM sodium orthovanadate, 10 mM sodium pyrophosphate, and 1 mM phenylmethylsulfonyl fluoride), measured by the Bradford assay (50), reduced with 5 mM DTT (56 °C, 25 min), alkylated in 14 mM iodoacetamide for 30 min in the dark, and quenched by DTT. The protein mixtures were diluted in 50 mM Tris-HCl (pH 8.8), digested by Lys-C overnight at 25 °C, desalted using an OASIS HLB 1-ml Vac cartridge (Waters), and subjected to TMT six-plex labeling. After TMT labeling, all samples were combined and lyophilized.

Strong cation-exchange fractionation—The peptide mixture was fractionated using a cation ion-exchange column (2.1-mm internal diameter × 20 cm packed with Poros 10 S, Dionex, Sunnyvale, CA) with an UltiMate® 3000 HPLC system at a flow rate of 200 μl/min using buffer A (7 mM KH_2PO_4 (pH 2.65) and 30% ACN) and buffer B (7 mM KH_2PO_4, 350 mM KCl (pH 2.65), and 30% ACN) in the following gradient: 0- 8% B in 0.1 min, 8–20% B for 15.9 min, 20–40% B for 20 min, 40–100% B for 1 min, 100% B for 5 min, 100–0% B in 1 min, 0% B for 25 min. Fractions were collected every 1.5 min.

LC-MS^3 analysis—29 fractions were separated by a reverse-phase microcapillary column (0.075 × 150 mm, Acclaim® PepMap100 C_{18} column, 3 μm, 100 Å; Dionex) using 2% ACN and 0.5% acetic acid (buffer A) and 80% ACN and 0.5% acetic acid (buffer B) under a 222-min gradient (3% buffer B for 10 min, 3–5% buffer B for 3 min, 5–20% buffer B for 167 min, 20–36% buffer B for 15 min, 36–100% buffer B for 1 min, 100% buffer B for 7 min, 100–3% buffer B for 1 min, 3% buffer B for 18 min) and analyzed using an LTQ Orbitrap Velos (Thermo Finnigan, San Jose, CA) with a higher-energy collisional dissociation MS^3 method.

Protein identification and quantification—The raw files were processed with MaxQuant software (version 1.2.2.5) using the UniProt mouse protein database (55,269 sequences). A common contaminants database was also included for quality control. The reverse strategy was used to estimate the false discovery rate. Except for TMT labels, carbamidomethyl (Cys) was set as fixed modification. Variable modifications were oxidation (Met) and acetyl (protein N terminus). The site, peptide, and protein false discovery rates were all set to 0.01. Protein quantification was calculated by combining MaxQuant identification results with a local modified Libra algorithm (49). For the identification of differentiated expressed proteins among groups, the cutoffs of -fold change and p value (Student's t test) were set to 1.5 and 0.05, respectively.

The MS proteomics data have been deposited to the ProteomeXchange Consortium (www.proteomexchange.org) via the PRIDE partner repository with the data set identifier PXD012579. The analyzed data are provided in Table S4.

Immunoprecipitation and GST pulldown assays

The full-length coding sequence (CDS) of *Stk40*, c-*Jun*, and *Cop1* were cloned into the pcDNA 3.0 vector, respectively. The truncated forms and mutants of *Stk40* and mutated c-*Jun* were also cloned into the pcDNA 3.0 vector, respectively. 293FT cells were seeded at 2×10^6 cells in 6-cm dishes on day 1, and 2 μg of expression vectors each or an empty vector were transfected with Lipofectamine 2000 reagent according to the manufacturer's instructions (Thermo Fisher Scientific) on day 2. After 24 h, cells were washed in the culture dish with cold PBS three times. Whole-cell lysates were prepared in co-IP buffer (50 mM Tris-HCl (pH 7.4) with 150 mM NaCl, 1 mM EDTA, 1% Triton X-100, and protease inhibitor mixture (Selleck)) and incubated with anti-FLAG M2 beads (Sigma) overnight at 4 °C. Then, beads were washed three times and eluted by 2× loading buffer for 10 min at 95 °C. For GST pulldown assays, the full-length *Stk40* CDS was cloned into the pGEX-4T-1 plasmid, and the full-length c-*Jun* and *Cop1* CDSs were cloned into the pET-30a(+) vector, respectively. GST and His fusion proteins were expressed in the BL21 strain and purified according to the manufacturers' instructions (GE Healthcare and Novagen). GST pulldown assays were performed as described previously (21). The samples from immunoprecipitation and GST pulldown were analyzed by Western blotting.

Flow cytometric analysis

GFP-Bry mESCs were infected with lentiviral particles that express shRNA. After puromycin selection (1 μg/ml), the remaining cells were subjected to induced differentiation toward mesoderm, and both GFP-positive and -negative cells were analyzed by flow cytometry.

Immunofluorescence staining

ESCs and differentiated cells were fixed with 4% paraformaldehyde at room temperature for 10 min, and immunostaining was performed as described previously (24). The mouse embryos were collected at E7.0, and whole-mount immunostaining was performed according to the iDISCO protocol (51). Images were captured using a confocal microscope (Leica TCS SP8). Primary antibodies used for immunostaining are provided in Table S3.

Protein stability assays with CHX

CHX (Sigma-Aldrich) was dissolved in DMSO at a concentration of 100 mM. Cells were cultured with CHX at a concentration of 50 μM for the indicated time. Then, cells were collected and subjected to Western blotting to visualize protein levels.

TOP/FOPFlash assays

8×TOPFlash or 8×FOPFlash and pRL-TK vectors (Promega) in combination with or without the WT or mutant (SSAA) c-*Jun* expression vector were transfected into 293FT cells with Lipofectamine 2000 reagent according to the manufacturer's instructions (Thermo Fisher Scientific). pRL-TK serves as a control to normalize the transfection efficiency. Twenty-four hours later, cells were treated with CHIR99021 (1 μM) for an additional 6 h and then lysed for luciferase assays. Luciferase activities were evaluated using a Dual-Luciferase Assay kit (Promega) according to the manufacturer's instructions. TOP/FOPFlash ratios are represented as mean ± S.D. ($n = 3$).

Statistical analysis

Data are presented as the mean ± S.D. from at least three independent experiments or samples. Statistical significance was analyzed by two-tailed Student's t test and is shown as follows: *, $p < 0.05$; **, $p < 0.01$; ***, $p < 0.001$.

Author contributions—J. H., B. L., and Y. J. conceptualization; J. H. resources; J. H. and Z. F. data curation; J. H., Z. F., M. S., Y. G., and X. G. software; J. H. formal analysis; J. H., H. Y., and B. L. investigation; J. H., S. L., F. X., L. G., F. T., J. G., H. Y., Y. G., X. G., and B. L. methodology; J. H., B. L., and Y. J. writing-original draft; J. H., S. L., X. S., L. W., F. X., and Y. J. project administration; J. H., B. L., and Y. J. writing-review and editing; H. Y. and Y. J. funding acquisition; Y. J. supervision.

Acknowledgment—We thank Dr. Gordon M. Keller for kindly providing the GFP-Bry mouse embryonic stem cell line.

References

1. Kojima, Y., Tam, O. H., and Tam, P. P. (2014) Timing of developmental events in the early mouse embryo. *Semin. Cell Dev. Biol.* **34,** 65–75 CrossRef Medline
2. Gadue, P., Huber, T. L., Nostro, M. C., Kattman, S. J., and Keller, G. (2005) Germ layer induction from embryonic stem cells. *Exp. Hematol.* **33,** 955–964 CrossRef Medline
3. Murry, C. E., and Keller, G. (2008) Differentiation of Embryonic Stem Cells to Clinically Relevant Populations: Lessons from Embryonic Development. *Cell* **132,** 661–680 CrossRef Medline
4. Liu, P., Wakamiya, M., Shea, M., Albrecht, U., Behringer, R. R., and Bradley, A. (1999) Requirement for Wnt3 in vertebrate axis formation. *Nat. Genet.* **22,** 361–365 CrossRef Medline
5. Lindsley, R. C., Gill, J. G., Kyba, M., Murphy, T. L., and Murphy, K. M. (2006) Canonical Wnt signaling is required for development of embryonic stem cell-derived mesoderm. *Development* **133,** 3787–3796 CrossRef Medline
6. Kelly, O. G., Pinson, K., and Skarnes, W. C. (2004) The Wnt co-receptors Lrp5 and Lrp6 are essential for gastrulation in mice. *Development* **131,** 2803–2815 CrossRef Medline
7. Wang, L., and Chen, Y. (2016) Signaling Control of Differentiation of Embryonic Stem Cells toward Mesendoderm. *J. Mol. Biol.* **428,** 1409–1422 CrossRef Medline
8. Angel, P., and Karin, M. (1991) The role of Jun, Fos and the AP-1 complex in cell-proliferation and transformation. *Biochim. Biophys. Acta* **1072,** 129–157 Medline
9. Shaulian, E., and Karin, M. (2002) AP-1 as a regulator of cell life and death. *Nat. Cell Biol.* **4,** E131–E136 CrossRef Medline
10. Eferl, R., and Wagner, E. F. (2003) AP-1: a double-edged sword in tumorigenesis. *Nat. Rev. Cancer* **3,** 859–868 CrossRef Medline
11. Liu, J., Han, Q., Peng, T., Peng, M., Wei, B., Li, D., Wang, X., Yu, S., Yang, J., Cao, S., Huang, K., Hutchins, A. P., Liu, H., Kuang, J., Zhou, Z., *et al.* (2015) The oncogene c-Jun impedes somatic cell reprogramming. *Nat. Cell Biol.* **17,** 856–867 CrossRef Medline
12. Gan, X. Q., Wang, J. Y., Xi, Y., Wu, Z. L., Li, Y. P., and Li, L. (2008) Nuclear Dvl, c-Jun, β-catenin, and TCF form a complex leading to stabilization of β-catenin–TCF interaction. *J. Cell Biol.* **180,** 1087–1100 CrossRef Medline
13. Nateri, A. S., Spencer-Dene, B., and Behrens, A. (2005) Interaction of phosphorylated c-Jun with TCF4 regulates intestinal cancer development. *Nature* **437,** 281–285 CrossRef Medline
14. Wei, W., Jin, J., Schlisio, S., Harper, J. W., and Kaelin, W. G. (2005) The v-Jun point mutation allows c-Jun to escape GSK3-dependent recognition and destruction by the Fbw7 ubiquitin ligase. *Cancer Cell* **8,** 25–33 CrossRef Medline
15. Gao, M., Labuda, T., Xia, Y., Gallagher, E., Fang, D., Liu, Y. C., and Karin, M. (2004) Jun turnover is controlled through JNK-dependent phosphorylation of the E3 ligase itch. *Science* **306,** 271–275 CrossRef Medline
16. Wertz, I. E., O'Rourke, K. M., Zhang, Z., Dornan, D., Arnott, D., Deshaies, R. J., and Dixit, V. M. (2004) Human de-etiolated-1 regulates c-Jun by assembling a CUL4A ubiquitin ligase. *Science* **303,** 1371–1374 CrossRef Medline
17. Vitari, A. C., Leong, K. G., Newton, K., Yee, C., O'Rourke, K., Liu, J., Phu, L., Vij, R., Ferrando, R., Couto, S. S., Mohan, S., Pandita, A., Hongo, J. A., Arnott, D., and Wertz, I. E., *et al.*(2011) COP1 is a tumour suppressor that causes degradation of ETS transcription factors. *Nature* **474,** 403–406 CrossRef Medline
18. Baert, J., Monte, D., Verreman, K., Degerny, C., Coutte, L., and de Launoit, Y. (2010) The E3 ubiquitin ligase complex component COP1 regulates PEA3 group member stability and transcriptional activity. *Oncogene* **29,** 1810–1820 CrossRef Medline
19. Uljon, S., Xu, X., Durzynska, I., Stein, S., Adelmant, G., Marto, J. A., Pear, W. S., and Blacklow, S. C. (2016) Structural basis for substrate selectivity of the E3 ligase COP1. *Structure* **24,** 687–696 CrossRef Medline
20. Migliorini, D., Bogaerts, S., Defever, D., Vyas, R., Denecker, G., Radaelli, E., Zwolinska, A., Depaepe, V., Hochepied, T., Skarnes, W. C., and Marine, J. C. (2011) Cop1 constitutively regulates c-Jun protein stability and functions as a tumor suppressor in mice. *J. Clin. Investig.* **121,** 1329–1343 CrossRef Medline
21. Li, L., Sun, L., Gao, F., Jiang, J., Yang, Y., Li, C., Gu, J., Wei, Z., Yang, A., Lu, R., Ma, Y., Tang, F., Kwon, S. W., Zhao, Y., Li, J., *et al.* (2010) Stk40 links the pluripotency factor Oct4 to the Erk/MAPK pathway and controls extraembryonic endoderm differentiation. *Proc. Natl. Acad. Sci. U.S.A.* **107,** 1402–1407 CrossRef Medline
22. Yu, H., He, K., Li, L., Sun, L., Tang, F., Li, R., Ning, W., and Jin, Y. (2013) Deletion of STK40 protein in mice causes respiratory failure and death at birth. *J. Biol. Chem.* **288,** 5342–5352 CrossRef Medline
23. Yu, H., He, K., Wang, L., Hu, J., Gu, J., Zhou, C., Lu, R., and Jin, Y. (2015) Stk40 represses adipogenesis through translational control of CCAAT/enhancer-binding proteins. *J. Cell Sci.* **128,** 2881–2890 CrossRef Medline
24. He, K., Hu, J., Yu, H., Wang, L., Tang, F., Gu, J., Ge, L., Wang, H., Li, S., Hu, P., and Jin, Y. (2017) Serine/threonine kinase 40 (Stk40) functions as a novel regulator of skeletal muscle differentiation. *J. Biol. Chem.* **292,** 351–360 CrossRef Medline
25. Wang, L., Yu, H., Cheng, H., He, K., Fang, Z., Ge, L., Cheng, T., and Jin, Y. (2017) Deletion of Stk40 impairs definitive erythropoiesis in the mouse fetal liver. *Cell Death Dis.* **8,** e2722 CrossRef Medline
26. Durzynska, I., Xu, X., Adelmant, G., Ficarro, S. B., Marto, J. A., Sliz, P., Uljon, S., and Blacklow, S. C. (2017) STK40 is a pseudokinase that binds the E3 ubiquitin ligase COP1. *Structure* **25,** 287–294 CrossRef Medline

27. Chal, J., Oginuma, M., Al Tanoury, Z., Gobert, B., Sumara, O., Hick, A., Bousson, F., Zidouni, Y., Mursch, C., Moncuquet, P., Tassy, O., Vincent, S., Miyanari, A., Bera, A., Garnier, J. M., *et al.* (2015) Differentiation of pluripotent stem cells to muscle fiber to model Duchenne muscular dystrophy. *Nat. Biotechnol.* **33,** 962–969 CrossRef Medline
28. Kazanskaya, O., Glinka, A., del Barco Barrantes, I., Stannek, P., Niehrs, C., and Wu, W. (2004) R-Spondin2 is a secreted activator of Wnt/β-catenin signaling and is required for *Xenopus* myogenesis. *Dev. Cell* **7,** 525–534 CrossRef Medline
29. Fehling, H. J., Lacaud, G., Kubo, A., Kennedy, M., Robertson, S., Keller, G., and Kouskoff, V. (2003) Tracking mesoderm induction and its specification to the hemangioblast during embryonic stem cell differentiation. *Development* **130,** 4217–4227 CrossRef Medline
30. Gadue, P., Huber, T. L., Paddison, P. J., and Keller, G. (2006) Wnt and TGF-β signaling are required for the induction of an *in vitro* model of primitive streak formation using embryonic stem cells. *Proc. Natl. Acad. Sci. U.S.A.* **103,** 16806–16811 CrossRef Medline
31. Gouti, M., Delile, J., Stamataki, D., Wymeersch, F. J., Huang, Y., Kleinjung, J., Wilson, V., and Briscoe, J. (2017) A gene regulatory network balances neural and mesoderm specification during vertebrate trunk development. *Dev. Cell* **41,** 243–261.e7 CrossRef Medline
32. Hartl, M., Bader, A. G., and Bister, K. (2003) Molecular targets of the oncogenic transcription factor jun. *Curr. Cancer Drug Targets* **3,** 41–55 CrossRef Medline
33. Jochum, W., Passegué, E., and Wagner, E. F. (2001) AP-1 in mouse development and tumorigenesis. *Oncogene* **20,** 2401–2412 CrossRef Medline
34. Dérijard, B., Hibi, M., Wu, I. H., Barrett, T., Su, B., Deng, T., Karin, M., and Davis, R. J. (1994) JNK1: a protein kinase stimulated by UV light and Ha-Ras that binds and phosphorylates the c-Jun activation domain. *Cell* **76,** 1025–1037 CrossRef Medline
35. Bianchi, E., Denti, S., Catena, R., Rossetti, G., Polo, S., Gasparian, S., Putignano, S., Rogge, L., and Pardi, R. (2003) Characterization of human constitutive photomorphogenesis protein 1, a RING finger ubiquitin ligase that interacts with Jun transcription factors and modulates their transcriptional activity. *J. Biol. Chem.* **278,** 19682–19690 CrossRef Medline
36. Xia, Y., Wang, J., Xu, S., Johnson, G. L., Hunter, T., and Lu, Z. (2007) MEKK1 mediates the ubiquitination and degradation of c-Jun in response to osmotic stress. *Mol. Cell. Biol.* **27,** 510–517 CrossRef Medline
37. Nateri, A. S., Riera-Sans, L., Da Costa, C., and Behrens, A. (2004) The ubiquitin ligase SCFFbw7 antagonizes apoptotic JNK signaling. *Science* **303,** 1374–1378 CrossRef Medline
38. Fang, D., and Kerppola, T. K. (2004) Ubiquitin-mediated fluorescence complementation reveals that Jun ubiquitinated by Itch/AIP4 is localized to lysosomes. *Proc. Natl. Acad. Sci. U.S.A.* **101,** 14782–14787 CrossRef Medline
39. Iakoucheva, L. M., Radivojac, P., Brown, C. J., O'Connor, T. R., Sikes, J. G., Obradovic, Z., and Dunker, A. K. (2004) The importance of intrinsic disorder for protein phosphorylation. *Nucleic Acids Res.* **32,** 1037–1049 CrossRef Medline
40. Downs, K. M., and Davies, T. (1993) Staging of gastrulating mouse embryos by morphological landmarks in the dissecting microscope. *Development* **118,** 1255–1266 Medline
41. Johnson, R. S., van Lingen, B., Papaioannou, V. E., and Spiegelman, B. M. (1993) A null mutation at the c-jun locus causes embryonic lethality and retarded cell growth in culture. *Genes Dev.* **7,** 1309–1317 CrossRef Medline
42. Herschman, H. R. (1991) Primary response genes induced by growth factors and tumor promoters. *Annu. Rev. Biochem.* **60,** 281–319 CrossRef Medline
43. Huelsken, J., Vogel, R., Brinkmann, V., Erdmann, B., Birchmeier, C., and Birchmeier, W. (2000) Requirement for β-catenin in anterior-posterior axis formation in mice. *J. Cell Biol.* **148,** 567–578 CrossRef Medline
44. Huttlin, E. L., Bruckner, R. J., Paulo, J. A., Cannon, J. R., Ting, L., Baltier, K., Colby, G., Gebreab, F., Gygi, M. P., Parzen, H., Szpyt, J., Tam, S., Zarraga, G., Pontano-Vaites, L., Swarup, S., *et al.* (2017) Architecture of the human interactome defines protein communities and disease networks. *Nature* **545,** 505–509 CrossRef Medline
45. Li, S., Xiao, F., Zhang, J., Sun, X., Wang, H., Zeng, Y., Hu, J., Tang, F., Gu, J., Zhao, Y., Jin, Y., and Liao, B. (2018) Disruption of OCT4 ubiquitination increases OCT4 protein stability and ASH2L-B-mediated H3K4 methylation promoting pluripotency acquisition. *Stem Cell Rep.* **11,** 973–987 CrossRef Medline
46. Ying, Q. L., Wray, J., Nichols, J., Batlle-Morera, L., Doble, B., Woodgett, J., Cohen, P., and Smith, A. (2008) The ground state of embryonic stem cell self-renewal. *Nature* **453,** 519–523 CrossRef Medline
47. Patro, R., Duggal, G., Love, M. I., Irizarry, R. A., and Kingsford, C. (2017) Salmon provides fast and bias-aware quantification of transcript expression. *Nat. Methods* **14,** 417–419 CrossRef Medline
48. Love, M. I., Huber, W., and Anders, S. (2014) Moderated estimation of fold change and dispersion for RNA-seq data with DESeq2. *Genome Biol.* **15,** 550–550 CrossRef Medline
49. Wen, F. P., Guo, Y. S., Hu, Y., Liu, W. X., Wang, Q., Wang, Y. T., Yu, H. Y., Tang, C. M., Yang, J., Zhou, T., Xie, Z. P., Sha, J. H., Guo, X., and Li, W. (2016) Distinct temporal requirements for autophagy and the proteasome in yeast meiosis. *Autophagy* **12,** 671–688 CrossRef Medline
50. Bradford, M. M. (1976) A rapid and sensitive method for the quantitation of microgram quantities of protein utilizing the principle of protein-dye binding. *Anal. Biochem.* **72,** 248–254 CrossRef Medline
51. Renier, N., Wu, Z., Simon, D. J., Yang, J., Ariel, P., and Tessier-Lavigne, M. (2014) iDISCO: a simple, rapid method to immunolabel large tissue samples for volume imaging. *Cell* **159,** 896–910 CrossRef Medline